Application Note

Cancer Research

Agilent

Trusted Answers

Multiformat Analysis of Adherent Cell Migration

Integrating automated wound healing and single-cell tracking using quantitative imaging

Author

Ernest Heimsath, PhD,
Joe Clayton, PhD,
Agilent Technologies, Inc.

Abstract

Cell migration is a fundamental biological process that requires orthogonal measurement strategies to capture both collective and individual behaviors. Conventional scratch-wound healing assays are limited by manual variability, extracellular matrix (ECM) disruption, and poor reproducibility, while single-cell migration analyses often lack throughput. Here, we describe an automated workflow that integrates reproducible wound generation and collective cell migration analysis with kinetic, single-cell tracking using the Agilent BioTek Cytation 9 cell imaging multimode reader. These complementary assay formats enable robust quantification of wound closure and individual cell trajectories under physiologically relevant conditions. Together, this approach provides a scalable and reproducible framework for multidimensional analysis of cell migration and pharmacological response.

Introduction

Cell migration is a tightly regulated, multiscale process that enables tissue organization, immune surveillance, wound repair, and tumor dissemination.[1-3] Depending on biological context, cells may migrate collectively as coordinated groups, or individually as autonomous units, each mode governed by distinct physical interactions, signaling pathways, and responses to the microenvironment. Dissecting these behaviors in vitro is therefore essential for understanding normal physiology, disease progression, and therapeutic modulation.

The wound healing assay remains a cornerstone for studying collective migration due to its conceptual simplicity and direct measurement of coordinated movement.[4] However, manual implementation introduces substantial experimental variability, including inconsistent wound geometry, imprecise placement, and unintentional disruption of underlying ECM coatings. These constraints limit reproducibility and obscure subtle but biologically meaningful differences in migratory responses.

In contrast, assays that track individual cell movement provide mechanistic insight into motility, persistence, and response to chemical or structural cues, yet they are often performed separately from collective assays and may suffer from limited throughput or analyst-dependent bias. As a result, reliance on a single migration modality can yield incomplete or misleading interpretations of cellular behavior.

To more faithfully model migration dynamics and capture complementary dimensions of motility, integrated workflows are needed that combine standardized assay execution, long-term kinetic imaging, and quantitative analysis across both population-level and single-cell scales. Automated platforms that unify these capabilities offer a path toward higher reproducibility, increased scalability, and more comprehensive characterization of cell migration in physiologically relevant in vitro systems.

Experimental

Cell lines

HT-1080 fibrosarcoma cells (part number CCL-121) and MCF10A non-tumorigenic mammary gland epithelial cells (part number CRL-10317) were purchased from ATCC (Manassas, VA). Derivative cell lines stably expressing a nuclear-localized GFP fluorescent protein (HT-1080) or nuclear-localized mKate2 fluorescent protein (MCF10A) were generated using eLenti-Green (part number 8711010) or eLenti-Red (part number 8711011), respectively, according to the manufacturer's guidelines (Agilent Technologies, Inc.; Santa Clara, CA).

Fibronectin ECM coating

Agilent 96-well imaging microplates (part number 204626) were treated with fibronectin (part number F1141; Sigma-Aldrich; Burlington, MA) diluted to 10 µg/mL in DPBS for 30 minutes, followed by three washes with DPBS before cell seeding.

Cell seeding

Adherent HT-1080 or MCF10A cell cultures were detached using TrypLE Express (part number 12605036; ThermoFisher Scientific; Waltham, MA), pelleted by centrifugation at 300 G, then resuspended in 1X DPBS. Cells were reseeded in 96-well plates at a density of 1×10^3 cells/well for random migration assays, and at a density of 2.5×10^4 cells/well for wound healing assays. Once seeded, cells were allowed to attach to the fibronectin-coated well bottom at room temperature (RT) for 30 minutes followed by overnight incubation at 37 °C.

Cytochalasin D treatment

Cytochalasin D (CytoD) is a potent mycotoxin that binds to the barbed end of actin filaments, inhibits their polymerization, ultimately impairing cell motility and migration.[5,6] Dilutions of CytoD were prepared in each cell line's respective media with a final eight-point dilution series: 1000, 316, 100, 31.6, 10, 3.16, 1, and 0 nM (Vehicle Control).

Agilent BioTek AutoScratch wound making tool

The wound healing assay was set up in Agilent 96-well imaging microplates using the Agilent BioTek AutoScratch wound making tool, which automatically creates reproducible scratch wounds in cell monolayers grown in microplates. The AutoScratch tool uses polytetrafluoroethylene (teflon) tips, which scrape away cell monolayers in a uniform wound width, which preserves the underlying EMC coating (in this study, fibronectin) compared to manually scratching the bottom of the well (Figure 3). Once the initial wound was created, subsequent wash steps were carried out using the Agilent BioTek MultiFlo FX multimode dispenser, which is a modular reagent dispenser with as many as two peristaltic pumps (eight-tube dispensers), two syringe pump dispensers, and a strip washer.

Kinetic imaging

Kinetic imaging of full 96-well plates was set to intervals of every 30 minutes for random migration assays, and hourly for wound healing assays for a total assay time of 18 hours. For both assays, a 4x (0.13 NA) objective was used to image high-contract brightfield and fluorescence channels (GFP for HT-1080 and Texas Red for MCF10A). Laser autofocus was engaged for both assay types using the endogenous nuclear fluorescence signal to establish the focal plane. These kinetic assays employed the Agilent BioTek BioSpa 8 automated incubator to maintain optimal culture conditions of 37 °C and 5% CO_2 while not actively imaging.

Image processing and cellular analysis

To ensure clarity, the procedures below are grouped into steps common to all assays and those unique to either the wound healing assay or the random migration assay.

- General image processing steps (all assays):
  - All image processing and analysis steps were performed using the Agilent BioTek Gen5 software.
  - The high-contrast brightfield channel was used for the initial kinetic alignment and data reduction step.
- Wound healing assay-specific analysis:
  The wound healing assay was adapted for a high-throughput, 96-well microplate format and was conducted as previously described[8,9] and as follows:
  - High-contrast brightfield channel images were used for cellular analysis.
  - Preprocessing background reduction (25 µm rolling ball) was applied to the high-contrast brightfield channel images with background set to Dark.
  - Cellular analysis was performed on the background-reduced (Tsf) image set with the following parameters:
    - Threshold: 1250
    - Background: Dark
    - Split touching objects: Deselected
    - Object selection size range: 500 to 100,000 µm²
    - Advanced detection: Image smoothing strength set to 20
- Kinetic cell area coverage values (Object Sum Area) were used to calculate wound closure over time using the formula:

$$C_t = \frac{(\text{Object Sum Area}_t - \text{Object Sum Area}_0) \times 100}{I_A - \text{Object Sum Area}_0}$$

  C_t is the percent wound confluence over time, Object Sum Area_t is the area covered by cells at each time point, Object Sum Area_0 is the area covered by cells at time 0, and I_A is the total image area.
- Random migration assay-specific analysis:
  The random migration assay adapted for a high-throughput, 96-well microplate format was conducted as previously described[7] and as follows:
  - Fluorescence channel images were used for cellular analysis.
  - Preprocessing background reduction (25 µm rolling ball) was applied to the fluorescence channel images (GFP for HT-1080, Texas Red for MCF10A).
  - Cell movement was measured by establishing a primary mask using the nuclear-localized fluorescent signal.
  - The Agilent BioTek Gen5 object tracking module was used with a search radius of 50 µm (approximately twice the nuclear diameter).
  - The minimum object life cycle was set to two frames to include all possible objects, and a subpopulation analysis further refined data to objects tracked for ≥ 18 hours.

Results and discussion

The AutoScratch wound making tool maintains ECM coat integrity while creating uniform wounds

The AutoScratch wound making tool is an automated tool that creates consistent and reproducible scratch wounds in cell monolayers formed on the bottom of a microplate well.[8,9] It can be configured with a manifold housing eight pins oriented such that each pin corresponds to each row of a 96-well microplate. Once initiated, the manifold positions itself over the first column of the microplate, lowers itself so the pins contact the cell monolayer, and creates a wound in the center of the well, which is repeated for all columns of the microplate (Figure 1).

The AutoScratch tool creates wounds in each well that are uniform in width and well position. A post-scratch wash step to remove cellular debris generated during scratch formation is necessary to achieve optimal assay results. This step can be conducted manually using a multichannel pipette or via the fully automated process developed for the MultiFlo FX multimode dispenser (Figure 2).

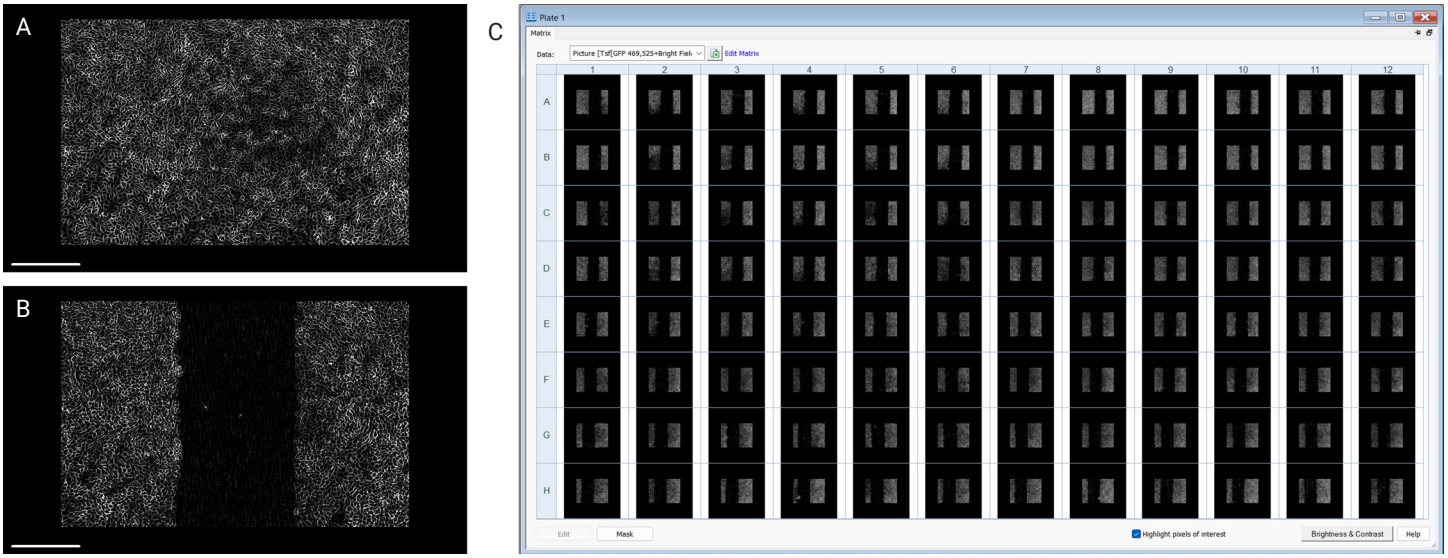

Figure 1. The Agilent BioTek AutoScratch wound making tool is an automated tool that creates consistent and reproducible scratch wounds. (A) Image of an HT-1080 monolayer before application of the AutoScratch wound making tool. (B) Image of the same well in (A) after wound generation with teflon tips. Scale bar = 500 µm. (C) Plate map view of a 96-well microplate demonstrating that wounds are consistent and reproducible.

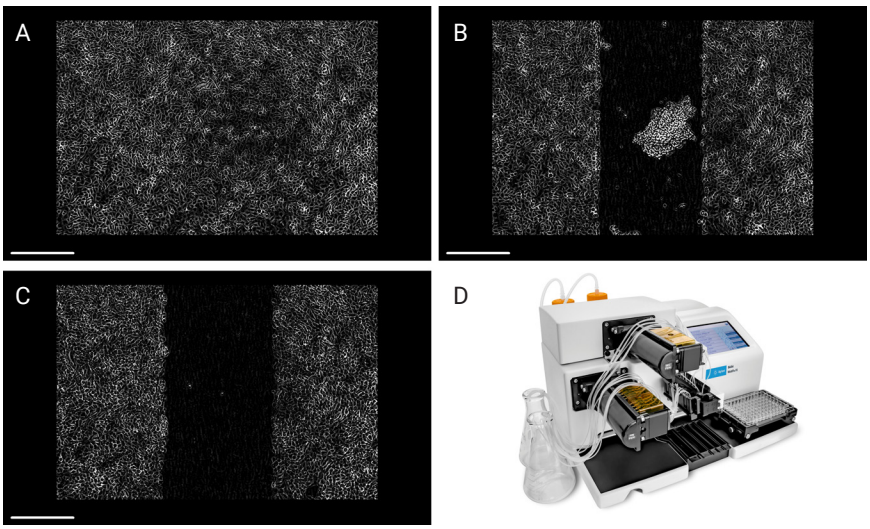

Figure 2. Removal of cellular debris from the Agilent BioTek AutoScratch wound making tool can be automated with the Agilent BioTek MultiFlo FX multimode dispenser. (A) A monolayer of HT-1080 cells before scratch generation. (B) The same well as (A) after application of the AutoScratch teflon pin. Note the cellular debris that remains and must be removed for accurate analysis, (C) The same well as (A) and (B) after automated washing with the MultiFlo FX (D). Scale bar: (A to C) = 500 µm.

Confirmation of AutoScratch compatibility with wound formation using ECM-coated microplates

The ECM provides a biologically relevant scaffold that facilitates cell migration and motility. As such, for the wound healing assay to mimic in vivo conditions, it is crucial that the ECM remains intact during wound formation. However, manual techniques for forming scratches are prone to disrupting and/or largely removing the ECM. To demonstrate the AutoScratch system's ability to generate accurate and reproducible wounds without disrupting the underlying ECM, fluorescently-labeled fibronectin (FITC) was used to coat the culture area of 96-well plates. A horizontal manual scratch was first created on the bottom of the well using a P200 pipette tip, which clearly disrupted the labeled fibronectin coating (Figure 3A). In contrast, a vertical scratch event was conducted to the same well using the AutoScratch tool (Figure 3B), demonstrating that the teflon material of the AutoScratch pins minimally disrupts the coated ECM.

HT-1080 and MCF10A exhibit distinct wound healing characteristics in response to the presence of fibronectin ECM and treatment with a known cytoskeletal disruptor

The Cytation 9 cell imaging multimode reader coupled with the Agilent BioTek BioSpa 8 automated incubator allows for expedient long-term imaging that captures the full-time course of the wound healing process. Combined with the AutoScratch tool, we performed a comparative analysis of the influence of ECM coating on the rate of wound closure. We observed that HT-1080 cells seeded on a fibronectin coating exhibit wound closure at a faster rate than when no underlying ECM is present (Figure 3C and D).

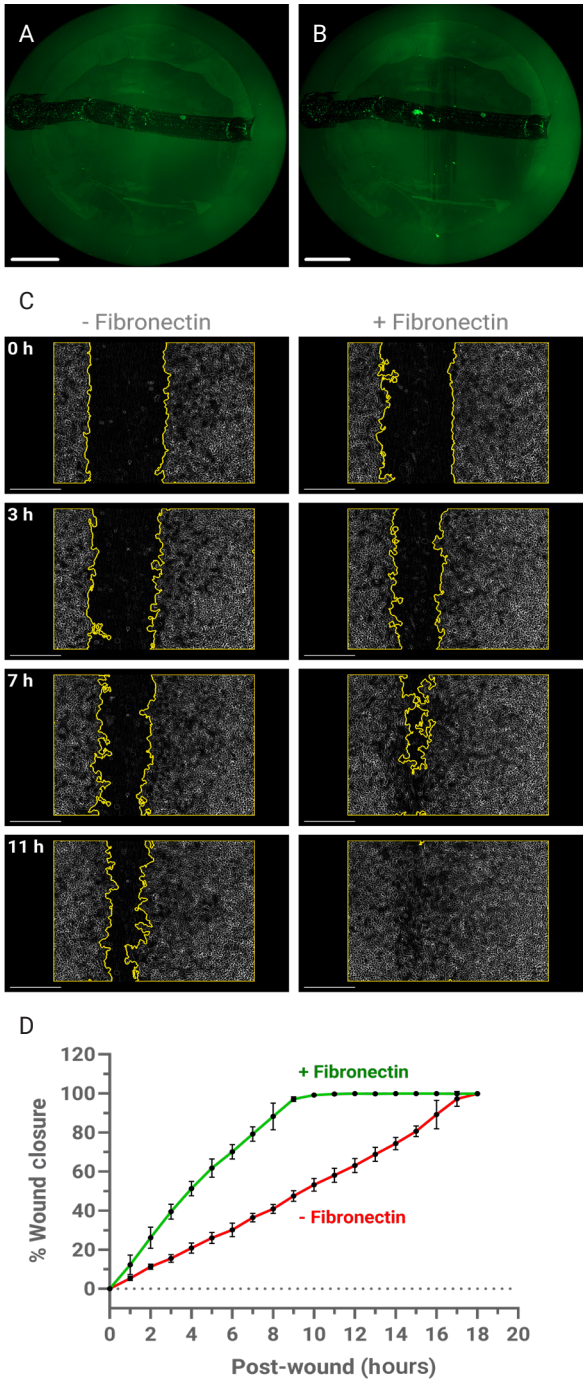

Figure 3. The Agilent BioTek AutoScratch wound making tool maintains fibronectin ECM coat integrity, which accelerates wound closure in HT-1080 cells. (A) Stitched image of a 2 x 2 montage of a 96-well microplate well coated with FITC fibronectin (green). A horizontal manual scratch was applied to the well, distrupting the coating. (B) The same well as (A) after application of the AutoScratch teflon pin. Scale bar = 1000 µm. (C) Selected timelapse frames depicting wound closure in a HT-1080 monolayer in the presence of (right) or absence (left) of 10 µg/mL fibronectin ECM precoating to microplate wells. Yellow lines indicate the masked areas used to quantify percent wound closure over the full timelapse indicated in (B). Scale bar = 500 µm. (D) Quantified comparison of wound closure rates of HT-1080 with (green) or without (red) a fibronectin ECM.

We next targeted the motile potential of HT-1080 by treating with a dilution series of cytochalasin D (CytoD), a potent mycotoxin that inhibits actin filament polymerization, resulting in well-characterized inhibition of cell motility and migration.[5,6] In the absence of a fibronectin ECM coating, HT-1080 cells have the potential to close a wound in a monolayer within an 18-hour assay window (Figure 4A), which is stunted by CytoD in a dose-dependent manner with an IC_{50} of 58.2 nM (Figure 4D). Under fibronectin-coated conditions, a faster HT-1080 wound closure rate was observed compared to non-coated conditions. However, HT-1080 wound closure rates retained a comparable sensitivity to CytoD inhibition with and without fibronectin coating when compared at their respective 100% wound closure time (Figure 4C and D).

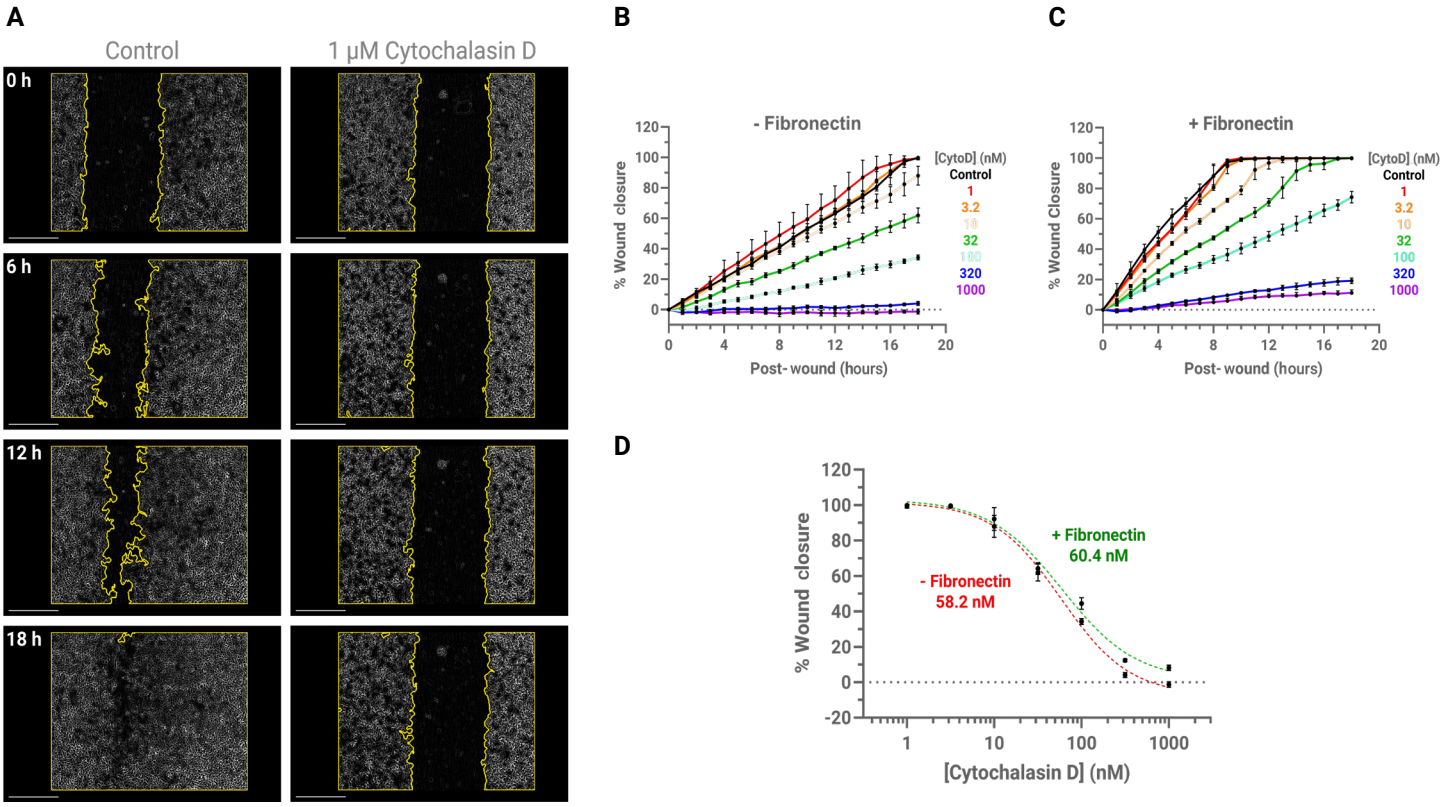

Figure 4. Cytochalasin D inhibits wound closure in HT-1080 cell monolayers. (A) Selected timelapse frames depicting wound closure in a HT-1080 monolayer in the presence of (right) or absence (left) of 1 mM cytochalasin D without an underlying fibronectin ECM. Scale bar = 500 µm. Yellow lines indicate the masked areas used to quantify percent wound closure over the full timelapse indicated in (B) no fibronectin ECM and (C) with fibronectin ECM, which is the duration for control to return to 100% closure. (D) Dose response of cytochalasin D on wound closure percentage of HT-1080 with or without the presence of an underlying fibronectin ECM at their respective 100% closure time in Control, with the indicated IC_{50}.

In addition to the HT-1080 fibroblast-based cell line, we successfully carried out wound healing assays with the MCF10A cell line, which is of epithelial origin. Interestingly, we observed that MCF10 wound closure rates are minimally affected by the presence of a fibronectin ECM coating (Figure 5A), and fibronectin did not appear to influence CytoD sensitivity (Figure 5B), although IC_{50} values are significantly higher with MCF10A than HT-1080 (Figures 4D and 5B).

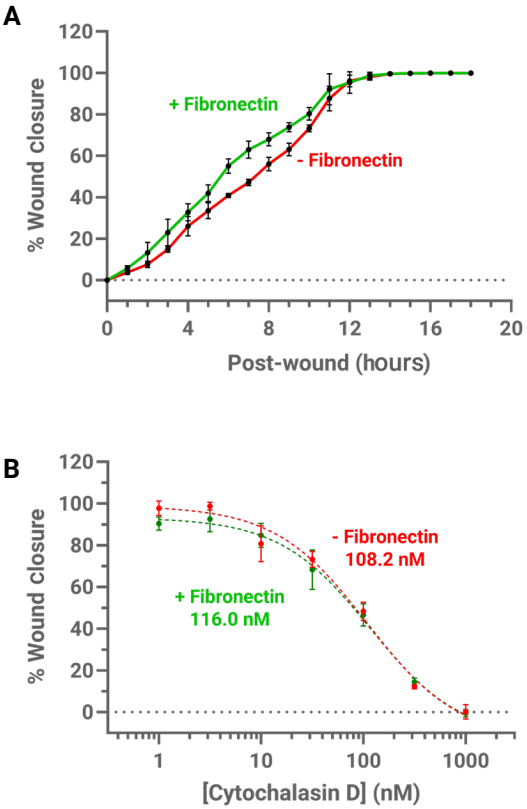

Figure 5. MCF10A epithelial cells maintain comparable wound closure rates and cytochalasin D sensitivity regardless of fibronectin ECM. (A) MCF10A mammary epithelial cells indicated no enhanced wound closure rates when seeded on a fibronectin ECM. (B) Comparison of cytochalasin D sensitivity on wound closure percentage of MCF10A with (green) or without (red) a fibronectin ECM at their respective 100% closure time, along with their indicated IC_{50} values.

ECM-dependent differences in single-cell migration between HT-1080 fibroblasts and MCF10A epithelial cells

In addition to collective migration measurements, random migration assays were performed to assess intrinsic single cell motility under ECM-modulated conditions. Using the Cytation 9 coupled with the BioSpa 8 automated incubator, time-lapse imaging was conducted in a 96-well microplate format, and migration velocities were quantified via Gen5 object tracking analysis. When evaluating the impact of fibronectin ECM undercoating alone, HT-1080 fibroblasts exhibited increased migration velocity on fibronectin-coated surfaces (19.7 µm/hr) compared to uncoated conditions (11.2 µm/hr), whereas MCF10A epithelial cells displayed reduced migration in the presence of fibronectin (24.1 µm/hr) relative to no ECM (33.5 µm/hr) (Figure 6). These findings indicate cell type specific differences in how ECM context modulates intrinsic migratory behavior.

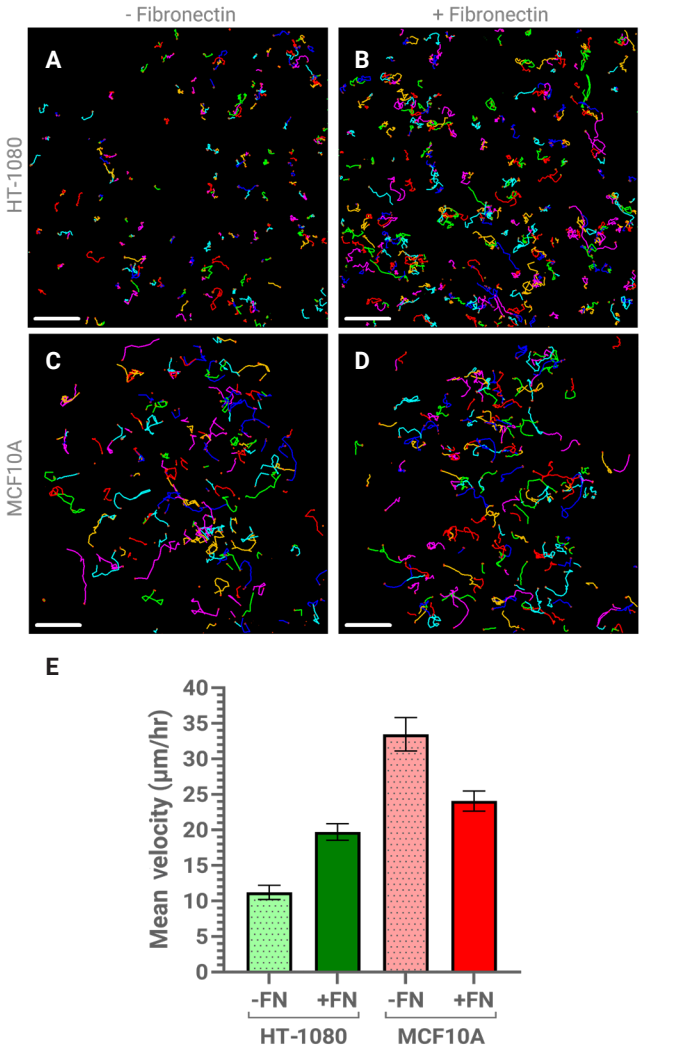

Figure 6. Influence of fibronectin ECM on random migration kinetic assay of HT-1080 and MCF10A cells. Migration tracks after 18 hours of HT-1080 cells (A and B) and MCF10A cells (C and D) in the absence or presence of fibronectin ECM. Scale bar = 500 µm. (E) Mean velocity rates of HT-1080 and MCF10A cells in the presence or absence of fibronectin ECM.

We next assessed migration responses to cytochalasin D under ECM-coated and uncoated conditions (Figure 7). For HT-1080 cells, enhanced migration on fibronectin corresponded with reduced sensitivity to inhibition, with the IC_{50} shifting from 149.2 nM without ECM to 223.8 nM on fibronectin (Figure 7E). In contrast, MCF10A cells demonstrated decreased migration velocity on fibronectin yet were less sensitive to inhibition under ECM coated conditions (IC_{50} = 243.0 nM) than without ECM (113.6 nM) (Figure 7F). Together, these results demonstrate that fibronectin ECM differentially regulates random migration kinetics and inhibitor sensitivity in fibroblast versus epithelial-derived cell lines, reinforcing the importance of ECM context when interpreting single-cell motility measurements.

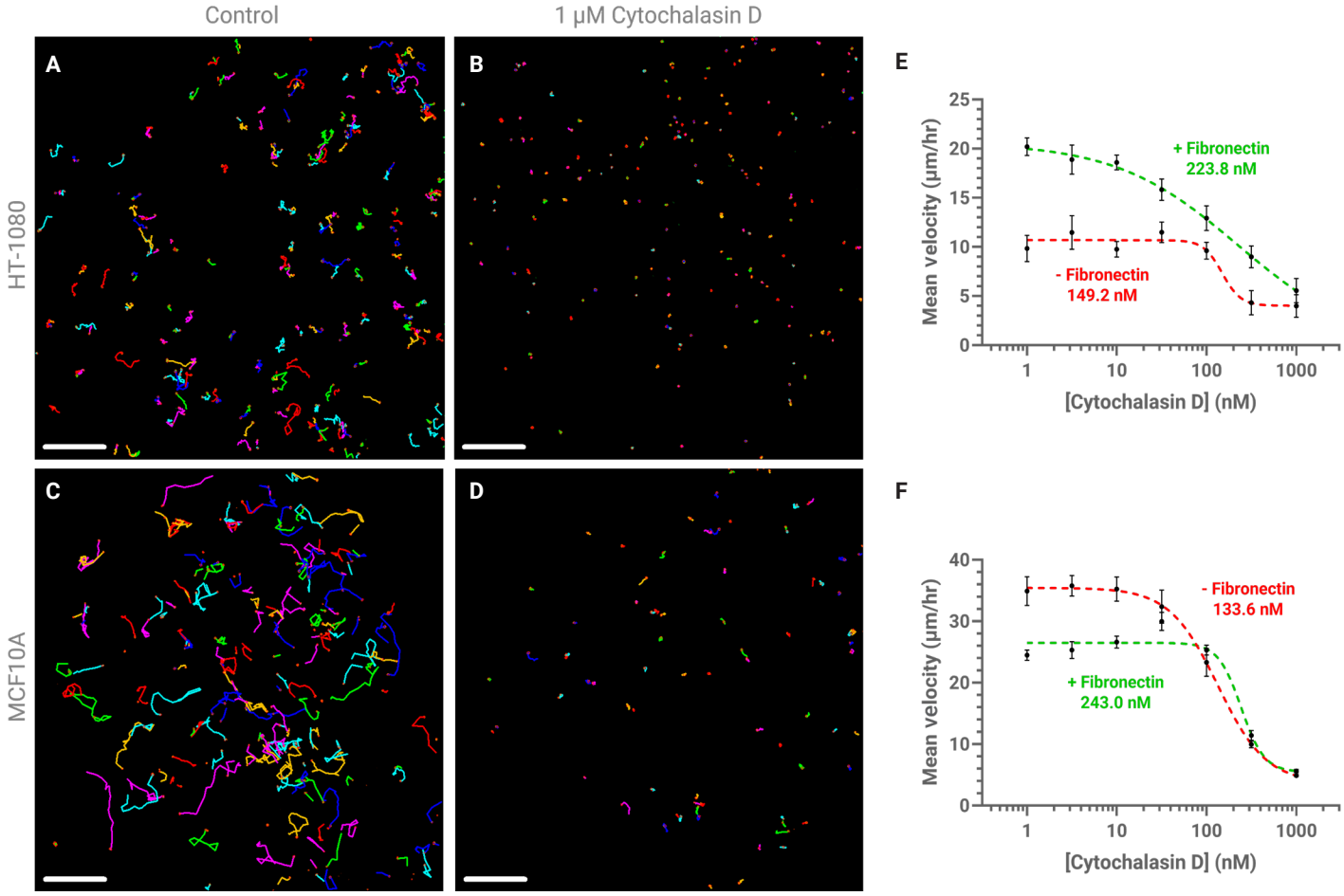

Figure 7. Random migration kinetic assay of HT-1080 and MCF10A cells. Migration tracks after 18 hours of HT-1080 cells (A and B) and MCF10A cells (C and D) in the absence or presence of 1 mM cytochalasin D. Scale bar = 500 µm. Dose response of cytochalasin D on mean velocity rates at 18 hours of HT-1080 (E) or MCF10A (F) in the presence or absence of fibronectin ECM, as indicated along with their respective IC_{50} values.

Conclusions

Cell migration is a multiscale, context-dependent process governed by distinct mechanisms underlying collective and single-cell behaviors. This application note demonstrates that combining orthogonal migration assays within a single workflow enables more comprehensive characterization of migratory phenotypes than reliance on any individual approach. By pairing automated wound healing assays with random migration analysis on the Agilent BioTek Cytation 9 cell imaging multimode reader, population-level coordination and intrinsic single-cell motility can be assessed side by side under matched experimental and analytical conditions.

Differences observed between fibroblast and epithelial-derived cell lines highlight the influence of cell identity and extracellular matrix engagement on migration behavior and pharmacological response. Divergent outcomes between wound closure and random migration measurements reinforce that metrics such as migration rate, coordination, and inhibitor sensitivity are assay and context dependent, underscoring the importance of interpreting results within the appropriate biological and microenvironmental framework.

Methodologically, integration of the Cytation 9 cell imaging multimode reader with the Agilent BioTek BioSpa 8 automated incubator enables stable, long-term kinetic imaging under controlled conditions, while standardized acquisition and analysis within the Agilent BioTek Gen5 software promote consistency and reproducibility across assays. The Agilent BioTek Gen5 object tracking module further supports robust quantification of individual cell trajectories, facilitating assessment of migratory behaviors governed by mechanisms distinct from collective migration. Together, these complementary capabilities provide a practical and reproducible framework for multidimensional analysis of cell migration in physiologically relevant in vitro models and for comparative evaluation of pharmacological perturbations.

References

1. SenGupta, S.; Parent, C.A.; and Bear, J.E. The Principles of Directed Cell Migration. *Nat Rev Mol Cell Biol* **2021**, *22*, 529–547. DOI: https://doi.org/10.1038/s41580-021-00366-6
2. Wu, C.; Asokan, S.B.; Berginski, M.E.; Haynes, E.M.; Sharpless, N.E.; Griffith, J.D.; Gomez, S.M.; and Bear, J.E. Arp2/3 Is Critical for Lamellipodia and Response to Extracellular Matrix Cues But Is Dispensable for Chemotaxis. *Cell* **2012**, *148*(5), 973987. DOI: https://doi.org/10.1016/j.cell.2011.12.034
3. Rotty, J.D.; Brighton, H.E.; Craig, S.L.; Asokan, S.B.; Cheng, N.; Ting, J.P.; and Bear, J.E. Arp2/3 Complex Is Required for Macrophage Integrin Functions But Is Dispensable for FcR Phagocytosis and In Vivo Motility. *Dev Cell* **2017**, *42*(5), 498–513. DOI: https://doi.org/10.1016/j.devcel.2017.08.003
4. Jonkman, J. E.; Cathcart, J. A.; Xu, F.; Bartolini, M. E.; Amon, J. E.; Stevens, K. M.; Colarusso, P. An Introduction to the Wound Healing Assay Using Live-Cell Microscopy. *Cell Adhes. Migr.* **2014**, *8*(5), 440–451. DOI: https://doi.org/10.4161/cam.36224
5. Carlier, M.F.; Criquet, P.; Pantaloni, D.; Korn, E.D. Interaction of Cytochalasin D with Actin Filaments in the Presence of ADP and ATP. *J Biol Chem.* **1986**, *261*(5):204–50. DOI: https://doi.org/10.1016/S0021-9258(17)35894-5
6. Hayot, C.; Debeir, O.; van Ham, P.; van Damme, M.; Kiss, R.; Decaestecker, C. Characterization of the Activities of Actin-Affecting Drugs on Tumor Cell Migration. *Toxicol Appl Pharmacol.* **2005**, *211*(1):30–40. DOI: https://doi.org/10.1016/j.taap.2005.06.006
7. Heimsath, E.G. Automated High-Throughput Imaging and Analysis of Cell Migration. Agilent Technologies, Inc. **2023**, 5994-5600EN.
8. Larson, B. Incorporation of a Novel, Automated Scratch Tool and Kinetic Label-Free Imaging to Perform Wound Healing Assays. Agilent Technologies, Inc. **2021**, 5994-2585EN.
9. Larson, B. Advanced Wound Healing Assay Workflow using Automated Scratch Wound Creation, High Contrast Brightfield and Fluorescence Kinetic Imaging. Agilent Technologies, Inc. **2021**, 5994-2397EN.

Products used in this application

Agilent products

BioTek Cytation 9 Cell Imaging Multimode Reader

BioTek AutoScratch Wound Making Tool

BioTek BioSpa 8 Automated Incubator

BioTek MultiFlo FX Multimode Dispenser

www.agilent.com/lifesciences/biotek

DE-014355

Published in the USA, April 29, 2026
5994-9152EN